Low Power UWB Transceivers for ISI Limited Environments: Design and Performance Verification

Florian Troesch and Armin Wittneben
Communication Technology Laboratory, ETH Zurich, 8092 Zurich, Switzerland
Email: {troeschf,wittneben}@nari.ee.ethz.ch

***Abstract*— Recently, we proposed an FCC compliant, ultra low power UWB transceiver based on binary pulse position modulation (BPPM) and a symbol-wise energy detector (ED) [1]. By means of a rigorous low duty cycle operation of 1% at a peak data rate of 50 Mbps, it features an average data rate of 500 kbps with a total average power below 1 mW. In this work, this symbol-wise ED is supplemented by a post-detector based on maximum likelihood sequence estimation (MLSE) which facilitates communication in inter-symbol interference (ISI) limited environments. A low complexity Viterbi detector, its metrics, as well as the required channel estimation is presented in a form which allows for direct implementation. Based on a complexity analysis, the additional power required by the post-detector is estimated. For practical scenarios, the overall transceiver power is still around 1 mW. Functionality of the modem design is verified by performance results obtained from an over-the-air testbed, which was operated in an ISI limited industrial environment.**

I. Introduction

Ultra-wideband impulse radio (UWB-IR) gained a lot of interest as an enabling technology for wireless sensor networks. Two areas of special interests are wireless body area networks (WBAN) and sensor, positioning and identification networks for industrial environments (SPIN). Both require ultra low power consumption of their nodes to guarantee a long battery autonomy.

For WBANs an ultra low power UWB-IR transceiver design was presented [1], which supports an average data rate of $R_{\text{Av}} = 500$ kbps at a total power consumption below 1 mW. Target bit error rate (BER) over an AWGN channel with path loss PL $= 60$ dB was BER $= 10^{-3}$. For complexity reasons, binary pulse position modulation (BPPM) and a symbol-wise energy detector (ED) is considered. To achieve a low power consumption, the average data rate of $R_{\text{Av}} = 500$ kbps is realized by burst-wise communication at a peak data rate of $R_{\text{P}} = 50$ Mbps and a 1% duty cycle operation of the mainly analog transceiver circuit. As typical delay spreads in WBANs are small, inter-symbol interference (ISI) was not an issue during the design process. Hence, the transceiver is vulnerable to it and performs bad in an ISI limited SPIN environment.

In this work, the symbol-wise ED receiver is supplemented by a post-detector which is based on maximum likelihood sequence estimation (MLSE). This enables ultra low power communication also in ISI limited environments. In contrast to existing ISI cancelation approaches, the proposed MLSE [2] works at the output of the ED frontend and takes into account the effect of non-linear cross-correlation terms. It equals a low complexity Viterbi decoder which operates at symbol rate, with very few states, and little channel state information (CSI). Its metrics are simplified based on the assumption of rectangular integration windows, which enables a Gaussian approximation of the non-linear noise terms. Due to the low complexity constraint, the energy integration in the frontend is realized by a first order low-pass (LP) and clearly does not meet this assumption. To enable the joint use of the MLSE post-detector and the low power transceiver frontend, a two-tap FIR filter is applied for equalization of the LP. The overall impulse response of LP and FIR is perfectly time-limited and almost rectangular. This enables direct application of the proposed low complexity MLSE post-detector. The resulting transceiver shows high ISI robustness at ultra low power.

The outline of the paper is as follows: After an overview of the low power frontend, the MLSE post-detector is introduced. Starting from the signal model at the output of the FIR filter, the Viterbi metrics are derived and channel estimation is discussed. The overall transceiver design including Viterbi metrics and channel estimation is presented in a form, which allows for direct implementation. Based on the metrics, the complexity of the post-detection is expressed in terms off additions (ADDs) and multiply-and-accumulates (MACs). This leads to stable power predictions of the post-detection as a function of register depth and over-sampling. They show that major parts of the power savings achieved by the low duty cycle operation are sustained also with MLSE post-detection. For practical SPIN scenarios, savings up to 97% are realized and enable a power consumption of the ISI robust, low power transceiver of about 1 mW. To demonstrate the effectiveness of the proposed MLSE post-detection, performance results are presented which were obtained from an over-the-air testbed operated in a typical SPIN environment. Performance gains of at least 4 dB in signal-to-noise ratio highlight a high potential.

II. System Proposal

The power consumption of UWB-IR transmitters is small compared to the one of the receivers [1]. Hence, focus is given to the receiver. The transmitter is modeled as a simple BPPM source transmitting bursts of 10μs every 1 ms at a peak data rate of 50 Mbps and an FCC compliant average transmit power of -14.26 dBm at 500 MHz.

A block diagram of the receiver chain is shown in Fig. 1. First, the received signal is amplified by a low noise amplifier (LNA) and bandpass filtered. Then, the signal is amplified by a variable gain amplifier (VGA), which is controlled by an

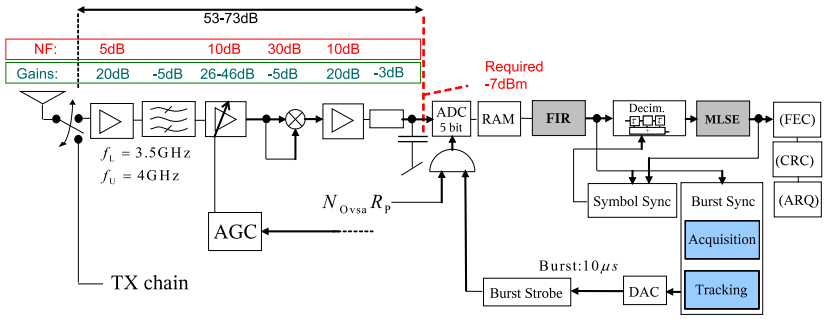

Fig. 1. Block diagram of UWB-IR receiver with MLSE post-detection

automatic gain control (AGC), squared and amplified again. For complexity reasons, the subsequent integration is realized by a simple first order low-pass. The LP output is sampled by a 5-bit analog-to-digital converter (ADC) with a free-running clock of $f_{\text{ADC}} = N_{\text{Ovsa}} R_{\text{P}}$ at an over-sampling of N_{Ovsa}. In the practical part, we set $N_{\text{Ovsa}} = 4$ [1]. The random-access memory (RAM) enables storage of a whole burst and burst-wise processing. In absence of MLSE post-detection, the RAM output is interpolated and down-sampled by the decimator, while the decoder consists of a simple subtraction. For MLSE post-detection two units are added. An FIR filter $g[k]$ to shape the integration window [3] and the actual MLSE decoder [2].

A. The Digital Filter

The proposed MLSE post-detector requires rectangular, strictly time-limited integration windows of duration $T = 1/f_{\text{ADC}}$. The LP impulse response is given by:

$$h_{\text{LP}}(t) \quad = \quad 1/T_0 e^{-t/T_0} \text{ for } t > 0, \text{ otherwise } 0, \qquad (1)$$

with $T_0 = (2\pi f_{\text{LP}})^{-1}$ and f_{LP}, the LP cut-off frequency. This is very different from the required integration window. However, a simple two-tap FIR filter $g[k]$ with $g[0] = 1$ and $g[1] = -\exp(-T/T_0)$ solves this problem very efficiently [3]. The concatenation of LP, ADC and FIR shows the input-output relation:

$$y[k] = \int_0^T q(kT - \tau) e^{-\tau/T_0} d\tau \overset{T_0 \gg T}{\approx} \int_{(k-1)T}^{kT} q(\tau) d\tau, \qquad (2)$$

with $q(t)$ the LP input. Accordingly, $y[k]$ is the kth output sample of an integration unit with perfectly time-limited integration window. For a sufficiently small bandwidth f_{LP}, the integration window approximates a rectangle due to $T_0 \gg T$ and $e^{-T/T_0} \approx 1$.

B. From Signal Model To Viterbi Structure

For derivation of the Viterbi metrics, a real discrete baseband model is used. Slow fading is considered and perfect synchronization is assumed. Non-linear amplifier characteristics are neglected. Furthermore, the PPM signal is expressed as PAM signal with the symbols $x_{2s} = b_s$ and $x_{2s+1} = 1 - b_s$ for $b_s \in \{0, 1\}$. A received burst of N_{Bits} bits is described by:

$$\begin{aligned} r[k] \quad &= \quad \sum_{s=0}^{N_{\text{Bits}}-1} x_{2s} h\left[k - sN\right] \\ &\quad + x_{2s+1} h\left[k - sN - N/2\right] + n\left[k\right], \end{aligned} \qquad (3)$$

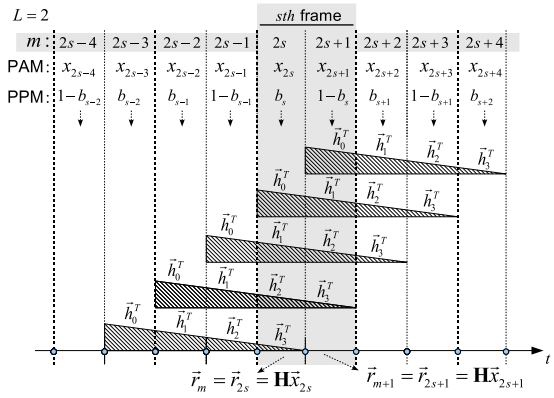

Fig. 2. Schematic construction of noiseless receive signal in the sth frame (half-slots: $2s$ and $2s + 1$) in case of $L = 2$

where N determines a frame and is assumed even. Both channel taps $h[k]$ and noise samples $n[k]$ are assumed to be mutually independent real Gaussian random variables. Introducing a half-frame index m, the notation simplifies to:

$$r[k] \quad = \quad \sum_{m=0}^{2N_{\text{Bits}}-1} x_m h\left[k - mN/2\right] + n\left[k\right]. \qquad (4)$$

Let the channel impulse response $\vec{h}$ comprise LN samples with $L \in \mathbb{N}$. Due to $LN > \frac{1}{2}N$ ISI occurs. As Fig. 2 illustrates for $L = 2$, the received signal in half-slot $2s$ is determined by $\vec{x}_{2s} = [x_{2s}, \ldots, x_{2s-3}]^T$. In half-slot $2s + 1$ in turn, the contributing PAM symbols are $\vec{x}_{2s+1} = [x_{2s+1}, \ldots, x_{2s-2}]^T$. From the figure follows that the received signal in both half-frames is completely determined by b_{s-2}, b_{s-1} and b_s. Independent of the preprocessing in the ED frontend, this set defines the states of the Viterbi decoder, while the preprocessing has impact on the branch metric, only. With the matrix

$$\begin{aligned} \mathbf{H} \quad &= \quad \left[\vec{h}_0, \vec{h}_1, \ldots, \vec{h}_{2L-1}\right] \qquad (5) \\ &= \quad \Big[\vec{h}\left[0 : N/2 - 1\right], \vec{h}\left[N/2 : N - 1\right], \ldots, \\ &\qquad \vec{h}\left[LN - N/2 : LN - 1\right]\Big], \qquad (6) \end{aligned}$$

the receive vector $\vec{r}_m$ in half-frame m follows to

$$\vec{r}_m \quad = \quad \mathbf{H}\vec{x}_m + \vec{n}_m, \qquad (7)$$

where $\vec{n}_m$ is a jointly Gaussian random vector with zero mean and $\mathcal{E}\{\vec{n}_m \vec{n}_m^T\} = \sigma^2 \mathbf{I}$. Schematically, the construction of $\vec{r}_m$ is indicated in Fig. 2.

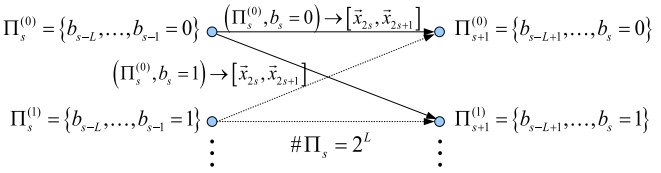

Fig. 3. Generic structure of the Viterbi decoder

The generic structure of the Viterbi is shown in Fig. 3. Unlike for a typical PAM signal, the depth of the state register Π_s equals L. This is because even a channel with $L = 1$ causes ISI, if the pulse is transmitted during the second half-frame. Hence, there are $|\Pi_s| = 2^L$ possible states per symbol. For $L = 2$, the Viterbi decoder has $2^L = 4$ states per symbol, corresponding to the four possible combinations of $\{b_{s-2}, b_{s-1}\}$. The state Π_s together with the symbol b_s, determine the vectors $\vec{x}_{2s}$ and $\vec{x}_{2s+1}$. Hence, they build the basis for the metric derivation at symbol index s.

C. The Viterbi Metrics as a Construction Plan

The ED frontend generates $\tilde{N}_{\text{Ovsa}} = N_{\text{Ovsa}}/2$ outputs per half-frame, whereby N_{Ovsa} is assumed even. To derive the signal contribution and the noise variance of the individual samples, appropriate submatrices of $\mathbf{H}$ are defined according to:

$$\begin{bmatrix} \vec{r}_{m,0} \\ \vec{r}_{m,1} \\ \vdots \\ \vec{r}_{m,\tilde{N}_{\text{Ovsa}}-1} \end{bmatrix} = \begin{bmatrix} \mathbf{H}^{(0)} \\ \mathbf{H}^{(1)} \\ \vdots \\ \mathbf{H}^{(\tilde{N}_{\text{Ovsa}}-1)} \end{bmatrix} \vec{x}_m + \vec{n}_m = \mathbf{H}\vec{x}_m + \vec{n}_m,$$

where $\mathbf{H}^{(k)}$ corresponds to the part of $\mathbf{H}$ which contributes to the kth set of samples within half-frame m. The kth ED output arising from the mth half-frame equals $y_{m,k} = \vec{r}_{m,k}^T \vec{r}_{m,k}$. Invoking the Gaussian approximation [2] and subtracting the non-linear bias term $\bar{z} = \mathcal{E}\left\{\vec{n}_m^T \vec{n}_m\right\}$ leads to:

$$d_{m,k} = \underbrace{\vec{r}_{m,k}^T \vec{r}_{m,k}}_{y_{m,k}} - \bar{z} = \underbrace{\vec{x}_m^T \left(\mathbf{H}^{(k)}\right)^T \mathbf{H}^{(k)} \vec{x}_m}_{\bar{d}_{m,k}} + \Delta z_{m,k}, \quad (8)$$

with the data dependent mean $\bar{d}_{m,k}$ and

$$\bar{z} = \frac{N}{2\tilde{N}_{\text{Ovsa}}}\sigma^2, \quad (9)$$

$$\Delta z_{m,k} \sim \mathcal{N}\left(0, \sigma_{\Delta z,s,k}^2\right), \quad (10)$$

$$\sigma_{\Delta z,m,k}^2 = \frac{N}{\tilde{N}_{\text{Ovsa}}}\sigma^4 + 4\vec{x}_m^T \left(\mathbf{H}^{(k)}\right)^T \mathbf{H}^{(k)} \vec{x}_m \sigma^2. \quad (11)$$

For each transition, the frontend provides $2\tilde{N}_{\text{Ovsa}}$ outputs $y_{s,k}$. The Viterbi subtracts the bias term according to $d_{s,k} = y_{s,k} - \bar{z}$ and builds the decision vector

$$\vec{d}_s = \left[d_{s,0}, \ldots, d_{s,2\tilde{N}_{\text{Ovsa}}-1}\right]^T, \quad (12)$$

with

$$d_{s,k} = \begin{cases} d_{m,k} & \text{for } 0 \le k \le \tilde{N}_{\text{Ovsa}} - 1 \\ d_{m+1,k-\tilde{N}_{\text{Ovsa}}} & \text{for } \tilde{N}_{\text{Ovsa}} \le k \le 2\tilde{N}_{\text{Ovsa}} - 1, \end{cases} \quad (13)$$

with $d_{m,k}$ and $d_{m+1,k}$ from (8). The elements $d_{s,k}$ are subject to statistically independent noise $\Delta z_{s,k}$. Their variance (11) is a function of the CIR and the PAM symbol vectors $\vec{x}_{2s}$ and $\vec{x}_{2s+1}$ associated with a specific transition. By normalizing each element $d_{s,k}$ to unit noise variance $\tilde{d}_{s,k} = \frac{d_{s,k}}{\sigma_{\Delta z,s,k}}$ with mean $\bar{\tilde{d}}_{s,k}$, Maximum Ratio Combining (MRC) according to:

$$\tilde{d}_s = \sum_{k=0}^{2\tilde{N}_{\text{Ovsa}}-1} \bar{\tilde{d}}_{s,k} \tilde{d}_{s,k}, \quad (14)$$

leads to a sufficient statistic of the decision vector $\vec{d}_s$. After some derivation steps, the Viterbi decoder follows to:

$$\underset{\bar{\tilde{d}}}{\text{argmin}} \sum_{s=0}^{N_{\text{Bits}}-1} \left(\hat{d}_s - \bar{\tilde{d}}_s\right)^2, \quad (15)$$

with

$$\bar{\tilde{d}}_s = \frac{1}{\|\vec{\bar{d}}_s\|} \sum_{k=0}^{2\tilde{N}_{\text{Ovsa}}-1} \frac{\bar{d}_{s,k}}{\sqrt{\frac{N}{\tilde{N}_{\text{Ovsa}}}\sigma^4 + \bar{d}_{s,k}}} \quad (16)$$

$$\hat{d}_s = \frac{1}{\|\vec{\bar{d}}_s\|} \sum_{k=0}^{2\tilde{N}_{\text{Ovsa}}-1} \frac{d_{s,k}}{\sqrt{\frac{N}{\tilde{N}_{\text{Ovsa}}}\sigma^4 + \bar{d}_{s,k}}}. \quad (17)$$

For $0 \le k \le \tilde{N}_{\text{Ovsa}} - 1$, the means are derived according to:

$$\bar{d}_{s,k} = \vec{x}_{2s}^T \left(\mathbf{H}^{(k)}\right)^T \mathbf{H}^{(k)} \vec{x}_{2s}, \quad (18)$$

and for $\tilde{N}_{\text{Ovsa}} \le k \le 2\tilde{N}_{\text{Ovsa}} - 1$, they equal:

$$\bar{d}_{s,k} = \vec{x}_{2s+1}^T \left(\mathbf{H}^{(k-\tilde{N}_{\text{Ovsa}})}\right)^T \mathbf{H}^{(k-\tilde{N}_{\text{Ovsa}})} \vec{x}_{2s+1}. \quad (19)$$

The norm is given by $\|\vec{\bar{d}}_s\| = \sqrt{\sum_{k=0}^{2\tilde{N}_{\text{Ovsa}}-1} \bar{d}_{s,k}}$.

D. Channel Estimation

Based on the Viterbi decoder described in (15), two different implementations are considered, which work with different CSI. The first Viterbi (MLSE-K) operates on the stacked impulse correlation matrix $\mathbf{K} = \text{diag}\{\mathbf{K}^{(0)}, \mathbf{K}^{(1)}, ..., \mathbf{K}^{(\tilde{N}_{\text{Ovsa}}-1)}\}$ built from block impulse correlation submatrices $\mathbf{K}^{(k)} = \left(\mathbf{H}^{(k)}\right)^T \mathbf{H}^{(k)}$. Each submatrix $\mathbf{K}^{(k)}$ has dimensionality $(2L \times 2L)$ and contains all energy and cross-correlation terms which possibly contribute to the kth decision element $d_{m,k}$ of any half-frame. In case of $\tilde{N}_{\text{Ovsa}} = 1$, $\mathbf{K}$ equals $\mathbf{K}^{(0)}$ with size $(2L \times 2L)$. Under the Gaussian assumption, the decision variable $\hat{d}_s$ of MLSE-K constitutes a sufficient statistics of the decision vector $\vec{d}_s$. The second Viterbi (MLSE-K_D) operates on the diagonal $\mathbf{K}_\text{D} = \text{diag}\{\mathbf{K}\}$ and ignores any cross-correlation terms.

To estimate $\mathbf{K}$ or $\mathbf{K}_\text{D}$ different pilot sequences are required. Assuming a noise-free receiver, the diagonal elements of $\mathbf{K}$ correspond to the output of the ED, if a single pulse is transmitted followed by $L-1$ idle frames. Accordingly, their estimation can be performed by transmission of a single pulse. To estimate the kth off-diagonal of $\mathbf{K}$, two pulses with delay

$kN/2$ are transmitted. The overall channel matrix $\mathbf{K}$ contains $\tilde{N}_{\text{Ovsa}}\left(2L^2+L\right)$ different elements. Its estimation requires $2L$ different pilot sequences. With $\mathbf{K}_{\text{D}}$ the estimation effort is drastically smaller. The diagonal matrix $\mathbf{K}_{\text{D}}$ contains only $\tilde{N}_{\text{Ovsa}}2L$ elements, which can be estimated based on a single pilot sequence.

III. Power Consumption

A. Symbol-wise Detector

Due to a constant supply voltage V_{DD}, the average power $P_{\text{Av}} = V_{\text{DD}}I_{\text{Av}}$ of the transceiver scales linearly with the average current consumption. This can be described as a linear function of the duty cycle $\eta \in [0,1]$ according to [1]:

$$I_{\text{Tot}}(\eta) \quad = \quad I_{\text{Digital}} + \eta I_{\text{Analog}}. \tag{20}$$

While the current consumption of the digital circuit is unaffected by the duty cycle, the current consumption of the analog circuit scales linearly with it. The analog current follows from the individual contributions of LNA, amplifiers, squarer, ADC and clock. Based on a meta study of existing current devices, it was estimated to $\eta I_{\text{Analog}} = 24.5$ mA at $\eta = 1$ and $\eta I_{\text{Analog}} = 0.24$ mA at $\eta = 0.01$ [1]. In absence of MLSE post-detection, the current consumption in the digital part is determined by the RAM and the synchronization. Assuming a linear current scaling with over-sampling, it was estimated to $I_{\text{Digital}} = 0.48N_{\text{Ovsa}}$ μA [1]. For the modem at hand and $N_{\text{Ovsa}} = 2\tilde{N}_{\text{Ovsa}} = 4$, this results in $I_{\text{Digital}} = 192$ μA.

B. MLSE Post-Detector

To derive the power consumption of the post-detection, a complexity estimation in terms of MACs and ADDs is performed starting from the Viterbi construction plan in Section II-C. Due to slow fading, the matrix $\mathbf{K}$ and the set of hypotheses $\hat{\tilde{d}}_s$ have to be updated only sparsely in time. With respect to average power these updates can be neglected. Only the FIR $g[k]$ and the construction of $\hat{\tilde{d}}_s$ have to be considered. The two-tap FIR can be realized by a single MAC per sample. Its complexity per bit equals $C_{\text{MAC,FIR}} = N_{\text{Ovsa}}$MAC/bit. For each transition of the Viterbi the samples are processed according to (17). Based on $d_{s,k}$ this corresponds to a simple FIR operation, while pre-factor and denominator are taken from memory. This requires $C_{\text{MAC,Metric}} = N_{\text{Ovsa}}$ MAC/metric. For the subtractions according to $d_{s,k} = y_{s,k} - \bar{z}$, $C_{\text{ADD,Metric}} = N_{\text{Ovsa}}$ ADD/metric are required. Depending on the register depth L, the Viterbi has 2^L states. Hence, to move from frame s to frame $s+1$ the Viterbi evaluates 2^{L+1} transition metrics and requires 2^L add-compare-select (ACS) units. They add the transition metrics to the overall paths and select the best one. According to [4], a ACS is modeled by $C_{\text{ADD,ACS}} = 3$ ADDs (2 addition and 1 comparison). The complexity of the Viterbi follows to:

$$C_{\text{ADD,Bit}} = 2^{L+1}C_{\text{ADD,Metric}} + 2^L C_{\text{ADD,ACS}} \text{ ADD/bit} \tag{21}$$

$$C_{\text{MAC,Bit}} = 2^{L+1}C_{\text{MAC,Metric}} \text{ MAC/bit.} \tag{22}$$

Both $C_{\text{ADD,Bit}}$ and $C_{\text{MAC,Bit}}$ grow linearly with over-sampling factor N_{Ovsa} and exponentially with L. Assuming a linear power scaling with clock frequency, the current consumptions for MAC and ADD operations, including read and write operations, is estimated to $I_{\text{MAC}} = 13.4$ μA/MHz and $I_{\text{ADD}} = 190$ nA/MHz, respectively [1]. Recalling N_{Bits} as the number of bits per burst, the average current consumption of FIR and MLSE follow to:

$$I_{\text{FIR}}\left(N_{\text{Ovsa}}, L\right) \quad = \quad \left(C_{\text{MAC,FIR}}N_{\text{Bits}}I_{\text{MAC}}\right)\cdot\left(10^3\right) \tag{23}$$

$$I_{\text{MLSE}}\left(N_{\text{Ovsa}}, L\right) \quad = \quad \left(C_{\text{ADD,Bit}}N_{\text{Bits}}I_{\text{ADD}} + C_{\text{MAC,Bit}}N_{\text{Bits}}I_{\text{MAC}}\right)\cdot\left(10^3\right). \tag{24}$$

C. Overall Current Consumption

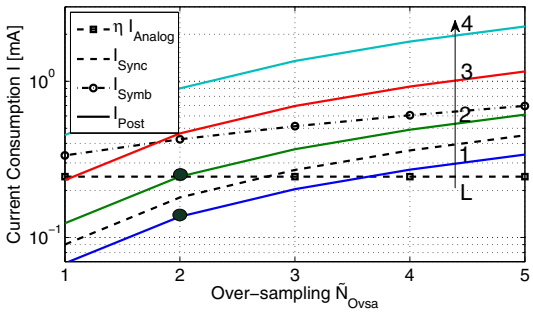

Fig. 4. Analog and digital receiver currents.

Fig. 4 shows the currents as a function of over-sampling $\tilde{N}_{\text{Ovsa}} = N_{\text{Ovsa}}/2$. The current consumption of the analog part ηI_{Analog} is independent of it and therefore constant. I_{Sync} and I_{Symb} equal digital and total current consumption of the symbol-wise detector, respectively. They scale linearly with over-sampling. For $\tilde{N}_{\text{Ovsa}} = 2$, the overall current consumption equals $I_{\text{Symb}} = 0.44$ mA. I_{Post} indicates the additional current for MLSE post-detection. It also scales linearly with over-sampling but exponentially with register depth L. Hence, only moderate register depths are feasible. However, $L = 2$ is generally sufficient for practical scenarios. At a peak data rate of $R_{\text{P}} = 50$ MHz, a Viterbi decoder with $L = 2$ equalizes excess delays up to 30 ns. E.g., the two black points in the figure indicate the operating points of the over-the-air performance evaluation presented in Section IV. At these points, MLSE post-detection increases the digital current consumption by at most 4 dB. The total receiver currents follow to $I_{\text{Rx,L=1}} = 0.57$ mA and $I_{\text{Rx,L=2}} = 0.68$ mA. Incorporating a current consumption of 0.6 mA for the duty cycled transmitter [1], the overall transceiver currents are $I_{\text{Sys,L=0}} = 0.5$ mA for symbol-wise detection and $I_{\text{Sys,L=1}} = 0.63$ mA and $I_{\text{Sys,L=2}} = 0.74$ mA for MLSE detection. For the provided ISI robustness, the moderate increase in current consumption seems a very attractive price. At a supply voltage of $V_{\text{DD}} = 1.5$ V, even the transceiver with $L = 2$ requires no more than 1.1 mW.

The ratio $\zeta(\eta) = E_{\text{Tot}}(\eta)/E_{\text{Tot}}(1)$ indicates the amount of energy, which can be saved by duty cycling and it strongly depends on the ratio between analog and digital current consumption [1]. For symbol-wise detection and a duty cycle of $\eta = 0.01$, it indicates power savings of 98%. For MLSE detection with $L = 2$ power savings at $\eta = 0.01$ are estimated

to 97%. This shows that major parts of the power savings achieved by a low duty cycle operation are maintained also with MLSE post-detection.

IV. Over-The-Air Performance

To demonstrate the effectiveness of the proposed MLSE post-detection, BER performance results are presented, which were obtained from an over-the-air testbed operated in a typical ISI limited SPIN environment. The main components of the testbed are a personal computer (PC), an arbitrary waveform generator (AWG), a digital sampling oscilloscope (DSO) as well as antennas and cables. On the PC, a MATLAB environment is running. It simulates the overall transceiver design using AWG and DSO as transmitting and receiving unit, respectively. Details about the testbed can be found in [5]. The realistic transceiver design is implemented according to the parameters in Section II and incorporates noise figures, amplifier non-linearities as well as channel estimation. Noise figures and amplifier gains are set according to Fig. 1. IIP3 points are set to $\mathrm{IIP3}_{\mathrm{LNA}} = -40$ dBm, $\mathrm{IIP3}_{\mathrm{VGA}} = -25$ dBm, and $\mathrm{IIP3}_{\mathrm{Amp2}} = 30$ dBm. The transmit power is limited to -14 dBm. After synchronization and channel estimation a total of 100800 bits is transmitted in bursts of 900 bits. For synchronization and channel estimation an additional burst is used. In case of MLSE post-detection, the LP bandwidth is set to $B_{\mathrm{LP}} = 20$ MHz. Together with the FIR this leads to a reasonably flat integration window. For symbol-wise detection a higher bandwidth improves performance. Hence, it is increased to $B_{\mathrm{LP}} = 100$ MHz.

The measurement environment equals a typical industrial working room with many metallic scattering objects such as machines and shelves. The size of the room is about 6×9 m. The antennas were mounted on tripods and placed in the middle of the room, 1.5 m above ground with LOS separation 1 m. To construct the NLOS scenario, the LOS component was blocked by a water tank. The path loss estimated from the peak amplitude of the LOS component was PL $= 52$ dB. The normalized cumulative energy functions (CEFs) of the CIRs are depicted in Fig. 5. They have significant energy components up to 30 ns and an MLSE performance improvement is expected for both. However, in case of LOS most of the energy is concentrated within the first 10 ns with a strong LOS component. In this case, it is expected that also the symbol-wise detector performs reasonable.

This is confirmed by the BER curves shown in Fig. 6. While in case of NLOS the symbol-wise detector fails completely, it works well in case of LOS. Once synchronized on the strong LOS component, the energy difference between the interval around the LOS component and the remaining part of the channel is sufficient to enable demodulation. All the same, MLSE post-detection brings gains of at least 4 dB. In case of LOS, ISI is moderate and the cross-terms in $\mathbf{K}$ are negligible. Hence, MLSE-$\mathrm{K_D}$ with drastically reduced channel estimation efforts performs similarly well as MLSE-K. This is different in case of NLOS. The lack of the LOS component increases the path loss and also causes synchronization mismatches. This

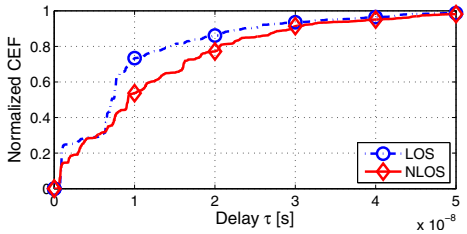

Fig. 5. Normalized CEF of the demonstration setups LOS and NLOS.

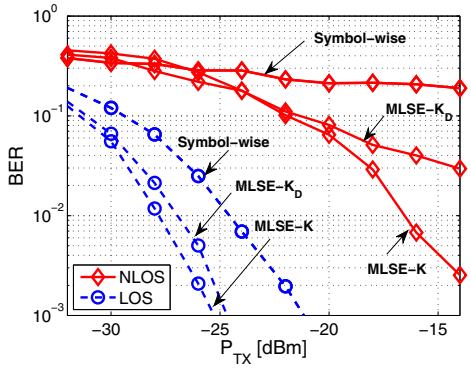

Fig. 6. BER performance in LOS and NLOS scenario.

increases the impact of ISI and the cross-correlation terms. Their neglecting leads to a drastic performance degradation and only MLSE-K shows a good performance. However, both applied Viterbi decoders operate with register depths $L \leq 2$ and their average power is below 1.1 mW. For the demonstrated ISI robustness, this seems acceptable.

V. Conclusions

An existing ultra low power transceiver design is extended by a low power MLSE post-detection to enable robust communication in ISI limited industrial environments. The overall transceiver design is presented in a form, which allows for direct implementation. The design is verified with respect to performance and power consumption. On the one hand, over-the-air simulation results verify its robust communication at 500 kbps in an ISI limited industrial environment. On the other hand, a complexity analysis of the Viterbi shows that this is accomplished at an average power consumption of about 1 mW. Hence, the presented transceiver design is a promising ultra low power transceiver for ISI limited environments.

References

[1] F. Troesch, C. Steiner, T. Zasowski, and A. Wittneben, "Hardware aware optimization of an ultra low power UWB communication system," in *IEEE Int. Conf. Ultra-Wideband (ICUWB)*, Marina Mandarin, Singapore, Sept. 24 – 26, 2007.

[2] F. Troesch, T. Zasowski, and A. Wittneben, "Non-linear UWB receivers with MLSE post-detection," in *IEEE Veh. Tech. Conf. (VTC)*, Pan Pacific, Sinapore, May 11–14, 2008.

[3] H. Luecken, T. Zasowski, and A. Wittneben, "Synchronization scheme for low duty cycle UWB impulse radio receiver," in *IEEE Int. Symp. Wirel. Comm. Sys.(ISWCS)*, Reykjavik, Iceland, Oct. 21–24, 2008.

[4] M. Leung, B. Nilolić, L. K.-C. Fu, and T. Jeon, "Reduced complexity sequence detection for high-order partial channels," *IEEE J. Select. Areas Commun.*, vol. 19, no. 4, Apr. 2001.

[5] C. Steiner, H. Luecken, T. Zasowski, F. Troesch, and A. Wittneben, "Ultra low power UWB modem design: Experimental verification and performance evaluation," in *XXIX General Assembly of the International Union of Radio Science (URSI)*, Chicago, IL, Aug. 7–16, 2008.